m-MTDATA on Au(111): Spectroscopic Evidence of Molecule–Substrate Interactions

T. Zhang,[1,] C. Grazioli,[2] A. Guarnaccio,[3] I. E. Brumboiu,[4] V. Lanzilotto,[5] F.O.L. Johansson,[6,7,8] Klára Beranová,[9,10] M. Coreno,[3] M. de Simone,[2] B. Brena,[6] and C. Puglia[6,*]*

[1] School of Integrated Circuits and Electronics, MIIT Key Laboratory for Low-Dimensional Quantum Structure and Devices, Beijing Institute of Technology, Beijing, China;

[2] IOM-CNR, Laboratorio TASC, Sincrotrone Trieste, 34149 Trieste, Italy;

[3] ISM-CNR, Istituto di Struttura della Materia, 85050 Tito Scalo, Pz, Italy

[4] Department of Chemistry, Pohang University of Science and Technology (POSTECH), 37673 Pohang, Republic of Korea;

[5] Department of Chemistry, Sapienza Università di Roma, P.le A. Moro 5, 00185 Roma, Italy;

[6] Department of Physics and Astronomy, Uppsala University, Box 516, SE-751 20 Uppsala, Sweden;

[7] Division of Applied Physical Chemistry, Department of Chemistry, KTH Royal Institute of Technology, 10044 Stockholm, Sweden;

[8] Institut des Nanosciences de Paris, UMR CNRS 7588, Sorbonne Université, F-75005 Paris, France.

[9] Elettra-Sincrotrone Trieste S. C. p. A., Strada Statale 14, km 163.5, Basovizza, Trieste 34149, Italy;

[10] FZU – Institute of Physics of the Czech Academy of Sciences, 18221 Prague, Czech Republic

Abstract

The starburst π-conjugated molecule based on triphenylamine (TPA) building blocks, 4,4′,4″-tris(*N*-3-ethylphenyl-*N*-phenylamino)triphenylamine ($C_{57}H_{48}N_4$, *m*-MTDATA), is widely used in optoelectronic devices due to its electron-donating properties. The electronic structure of *m*-MTDATA adsorbed on an Au(111) surface was investigated by means of photoelectron spectroscopy (PES) and near edge X-ray absorption fine structure (NEXAFS) spectroscopy. The results were further compared to gas-phase measurements and DFT calculations. Our results clearly indicate a significant molecule–substrate interaction that induces considerable modifications on the electronic structure of the adsorbate

compared to the isolated molecule. The energy level alignment analysis shows that the HOMO–LUMO gap is filled by new interface states.

Introduction

m-MTDATA (4,4′,4″-tris(*N*-3-methylphenyl-*N*-phenylamino)triphenylamine, $C_{57}H_{48}N_4$) belongs to a group of molecules called "starburst π-conjugated systems", for which the triphenylamine (TPA) is regarded as their building block (Figure 1). (1−8) Starburst molecules are quite often found in organic optoelectronic devices, like organic light emitting diodes (OLEDs), organic photovoltaics (OPVs), and more recently, solid dye sensitized solar cells (DSSCs), proving to be a key factor of their high efficiency. (9−13) Our study of gas-phase *m*-MTDATA (14) showed that the good electron-donating and charge-transfer properties of this starburst molecule are largely related to its building block triphenylamine (TPA), particularly involving the lone pair electrons of the N atoms. Moreover, the more complex molecular structure of *m*-MTDATA with respect to TPA potentially promotes the formation of homogeneous amorphous and glassy molecular films with higher thermal stability and better electron transport properties than films of TPA. (15−17)

Recent studies have shown that blends of electron-donating and electron-accepting molecules can improve significantly the performance of OPVs and OLEDs. (9−11,18−24) The performance of such devices is related both to the energy level matching between the donor and the acceptor components and to the charge transfer/separation occurring at the interfaces between the organic/inorganic semiconductors or between the donor and acceptor materials. For new developments and device optimizations, fundamental studies of the electronic structure of components (donor, acceptor) and of the electronic structure modifications occurring at the interfaces are therefore crucial for the understanding of the charge separation at organic/inorganic and organic/organic heterojunctions. (25)

In this study, we characterize the adsorption of *m*-MTDATA on an Au(111) surface by core and valence photoelectron spectroscopy (PES) and near-edge X-ray absorption fine structure (NEXAFS) spectroscopy. The comparison between different molecular depositions on Au(111) reveals that the geometrical arrangement of the molecules strongly depends on the coverage. Moreover, a strong modification of the molecular electronic structure compared to the isolated *m*-MTDATA, especially for the monolayer/interface and submonolayer case, is observed and is ascribed to the molecule/Au interaction. This will have important implications on the performance of the devices in which such materials are implemented.

Methods

Experimental Methods

The *m*-MTDATA thin film measurements were carried out at the Materials Science beamline of the Elettra Synchrotron. (26) The PE spectra were recorded by the Specs Phoibos 150 hemispherical electron analyzer mounted at the end station. During measurements, the base pressure of the analysis chamber was in the 10^{-10} mbar range. All the samples were prepared with a base pressure of high 10^{-10} mbar range. The clean Au(111) substrate was cleaned by repeated Ar^+ sputtering and annealing cycles until no contaminants were observed by PE measurements.

The *m*-MTDATA (Sigma-Aldrich, purity 98%) were deposited onto the clean Au(111) via thermal evaporation from a quartz crucible that was resistively heated to 190 °C by a tantalum wire. The thickness of the *m*-MTDATA films was controlled by the evaporation time and estimated by the attenuation of the PES Au 4f lines. We used multilayer samples (∼3 molecular layers), interface samples (∼1.3 molecular

layers), and low-coverage samples (~0.4 molecular layer) to shed light on the interfacial modifications to the electronic structure of *m*-MTDATA. Due to the Volmer–Weber (island) type growth of the *m*-MTDATA film (discussed later), it is difficult to achieve full monolayer coverage of *m*-MTDATA on an Au(111) substrate. Thus, the ~1.3 molecular layer sample was chosen to represent the monolayer sample of *m*-MTDATA/Au (i.e., the interface sample).

The C 1s and N 1s core level PE spectra were measured at normal emission (NE) with respect to the electron analyzer using photon energies of 392 and 495 eV, respectively. At these photon energies, the electron kinetic energy is close to the escape depth minimum and optimized to enhance surface sensitivity. The overall resolutions were about 330 and 430 meV for C 1s and N 1s, respectively, estimated from the width of the Fermi edge of the clean Au(111) crystal. Similarly, the overall resolution of the valence spectra measured with photon energies of 40 and 100 eV was about 150 meV, where the resolution using100 eV photon energy is slightly worse than when using 40 eV.

The NEXAFS spectra at the C and N K-edges of the deposited molecules were recorded using partial Auger yield. The measurements were performed at different scattering geometries: normal incidence (NI, 90° between the incident light and the surface plane), normal emission (NE, 90° between the analyzer and the surface plane or 60° between the incident light and the surface plane), and grazing incidence (GI, 10°, between the incident light and the surface plane). The photon energy scales of the NEXAFS were calibrated by measuring the Au 4f PES lines by the first- and second-order light. The energy resolution for the C and N K-edge NEXAFS spectra was estimated to be about 250 and 400 meV, respectively. The measured spectra were normalized to the intensity of the photon flux measured simultaneously on a high-transmission gold mesh. The C K-edge spectra were further normalized to the background spectra of the clean Au(111) surface, in order to eliminate spectral features due to the carbon contamination on the mesh and the beamline optics.

Computational Methods

The geometry of an isolated *m*-MTDATA molecule was optimized using the B3LYP (27) exchange and correlation functional in combination with the 6-31G(d,p) (28) basis set. The optimization was carried out in the Gaussian 16 (29) quantum chemistry software. An extensive characterization of *m*-MTDATA in the gas phase has been carried out in ref (14), and in the present work we refer to the notation adopted therein.

Results and Discussion

Structure of Isolated *m*-MTDATA

As shown in Figure 1, *m*-MTDATA contains 14 chemically nonequivalent C atoms and a total of 4 N atoms, which includes one central (N_C) and three peripherals (N_P). It is evident that the core of *m*-MTDATA is a TPA molecule (whose structure is shown in Figure 1c), which has a propeller-like form, with a torsion angle of 41.7° of the phenyl rings. (19) The *m*-MTDATA molecule has a more complicated structure, where the torsion angles of the phenyl rings connected to the central N (N_C) atom are approximately 41.7°, just like in TPA. However, the torsion angles related to the peripheral N (N_P) atoms are different since the local planes formed by the three C_{ipso} atoms with a N_P at the center, denoted [N_P–(C_{ipso})$_3$], are rotated with respect to the central [N_C–(C_{ipso})$_3$] plane by about 2.2–2.4° (see Figure 1b), even though all four N atoms sit in the same molecular plane, i.e. [(N)$_4$-plane]; see Figure 1a. Specifically, the average torsion angle

between each ring A and the [N_P–$(C)_3$] planes is 44.1°. The torsion angle between the [N_P–$(C_{ipso})_3$] planes and phenyl rings B are approximately 39.9°. Finally, the torsion angle between the [N_P–$(C_{ipso})_3$] planes and the phenyl rings C are 41.2°. These local torsions mean that the phenyl rings B are twisted by approximately 41.1° with respect to the molecular plane, i.e., $(N)_4$-plane, defined by the four N atoms. Similarly, the phenyl rings C are twisted by approximately 42.3° with respect to this molecular plane. We stress here that the structural characteristics described above are for the isolated *m*-MTDATA molecule and that the molecular geometry changes upon deposition on a substrate, as discussed below.

C 1s PES

The experimental and fitting of C 1s PE spectra of *m*-MTDATA in the gas phase and deposited on an Au(111) single crystal at different thicknesses are shown in Figure 2. Three samples of different coverages are analyzed, from low-coverage to interface to multilayer samples (see Experimental Methods). The fitting was performed by using Gaussian curves, and the results are presented in Table 1. The chemical shift between the main peak and the low-intensity peak is about 1 eV, similar to the gas-phase results. (14)

1. Multilayer Sample

We will start by analyzing the multilayer sample, where *m*-MTDATA keeps most of its molecular-like character (Figure 2b), confirmed by the line profile of the corresponding C 1s PE spectrum, which is very similar to the gas-phase results as further discussed in the following sections. The spectrum shows a high-intensity peak at 285.0 eV and a structure of lower intensity at about 285.5 eV on the higher being energy side. The spectrum has been fitted using two peaks. The intensity ratio of peak B vs peak B' is 2.8 as in the gas phase (A/A', Figure 2a), (14) in agreement with the stoichiometry of the isolated molecule. In detail, peak B' comes from methyl ($-CH_3$) and C_{ipso} atoms (directly bonded to the N atoms, −C–N−) while B comes from the other C atoms within the phenyl rings, i.e., 15/42 = 1/2.8.

As expected, for all the coverages the peaks of the C 1s PE spectrum (14) are broader than in the gas phase. Besides the common solid-state effect, (30) reasons for this can be the different geometries (disorder) that the adsorbed molecules can adopt in films on surfaces (as also confirmed later by C K-edge NEXAFS), which would result in even more chemically inequivalent atoms contributing at different BEs.

2. Interface and Low-Coverage Samples

For the C 1s PE spectra of the thinner films, i.e., interface and low coverage shown in Figure 2c,d, respectively, the peaks shift to lower BE, partly due to the more effective core-hole screening by the Au(111) surface, (31) even if we cannot exclude any initial-state effects. The C 1s spectrum of the low-coverage *m*-MTDATA/Au(111) sample is characterized by two peaks. One more intensive at 283.9 eV and the other one at 284.9 eV. This spectrum has been fitted by using two peaks, D and D'. For the low-coverage sample, the intensity ratio of peak D vs peak D' is only 1.25, deviating significantly from the stoichiometric value (2.8). This indicates a significant modification of the molecular structure with respect to the free molecule in Figure 1. The differences observed in the PE spectra can have many different origins. For example, there can be shifts due to direct interactions of the C atoms with the surface, the adsorption geometry may be very distorted with respect to the gas phase, or there may be diffraction effects which can alter the intensity ratios of the peaks.

For the interface sample, the spectral features are less resolved, but we still can distinguish a more intensive peak at 284.0 eV and the weaker one at about 284.9 eV. The fit reveals that the ratio between

the main and the shoulder peaks is different with respect to both the low-coverage and multilayer samples. We get a good fit of the interface C 1s spectrum only if we include the first and second layer components. After the decomposition, the intensity ratio of C1/C1′ of the first layer was found to be like that of the low-coverage sample, i.e., with a similar BE (shifted only +0.02 eV) and with a similar intensity ratio (1.2). The second layer components are shifted by +0.41 eV to higher BE (with respect to the first layer components) with an intensity ratio C2′/C2 of 2.6, more like the multilayer case. The fit seems to suggest that the second layer has already a molecular-like character. Although the spectrum of the interface sample clearly requires a second layer contribution, we note that the average thickness estimated from the attenuation method (32) is much less than a full coverage (only ∼1.7 Å). In view of this, it is reasonable to consider the growth of the *m*-MTDATA layer to be a Volmer–Weber (island) type from early stage of deposition instead of Stranski–Kastanov or Franck–van der Merwe growth, i.e., without the completion of full monolayers.

N 1s PES

The N 1s photoelectron spectra of *m*-MTDADA adsorbed on Au(111) at two coverages are shown in Figure 3. The N 1s BE is shifted from 399.30 eV (interface sample) to 399.90 eV (multilayer sample), likely due to the different core-hole screening for the two coverages as already observed for the C 1s spectra of the same samples. The N 1s line of the multilayer sample is slightly broader than the line of the interface sample (1.25 vs 0.99 eV), possibly related to the increased disorder in the multilayer film, as also later confirmed by N K-edge NEXAFS. The N 1s PE spectrum of the multilayer sample shows a broad low-intensity feature at about 7 eV from the main line, similar to the N 1s shakeup of TPA measured in the gas phase. (33) It is difficult to discern if such a feature is also present in the spectrum of the interface sample, due to the noisy signal.

C K-Edge NEXAFS

In Figure 4 we show the angle-dependent C K-edge NEXAFS spectra of the different coverages of *m*-MTDATA adsorbed on the Au(111) surface in comparison to the gas-phase results. (14) When the incident angle of the linearly polarized synchrotron light with respect to the surface is varied, i.e., from grazing incidence (GI, 10°) to normal incidence (NI, 90°), the cross-section of X-ray absorption of different orbitals, namely, for the π* (out-of-plane) or the σ* (in-plane) orbitals, varies, allowing us to investigate the orientation of the adsorbed molecules.

Both interface and multilayer samples do not show significant variation between π* and σ* orbital intensities at the different experimental setups. According to free molecule calculations, (14) there is an average twist angle of about 41–42° for all phenyl rings with respect to the horizontal molecular plane formed by the 4 N atoms, giving the molecule a very complex geometric structure (Figure 1). It is then difficult to draw any conclusions about the molecular orientation for the interface coverage.

The multilayer sample does not show significant variation between π* and σ* orbital intensities at the different experimental setups, while the interface sample does show dichroism. For the interface sample, the σ* orbitals did not change much from NI to GI, but the π* seems to respond more to the variation of the incident angle of the beam. We observe an enhancement of the π* resonances in GI, indicating a preferential ordering of some of the phenyl rings, i.e., more parallel to the surface. Indeed, from our previous study related to the isolated molecule, the first π* resonance (peak A, at 285.0 eV) is related to the contributions from all carbon atoms belonging to the phenyl rings with the exception of the carbons

directly bonded to nitrogen. (14) The second π* resonance, at higher photon energy (A', at 286.2 eV), is instead attributed to the C_{ipso} atoms (covalently bonded to the N atoms) and to the methyl ($-CH_3$) C atoms. Additionally, the adsorption of the building block molecule TPA on Au(111) shows a similar behavior of the C K-edge NEXAFS at monolayer coverage. (34)

The results of the multilayer sample are quite similar to the C K-edge NEXAFS of *m*-MTDADA in the gas phase, indicating that the phenyl rings of *m*-MTDATA in subsequent layers lose the preferential orientation characteristic of the interface sample and are rotated at different angles similarly to the free molecule structure, giving the layers a more "disordered" character.

N K-Edge NEXAFS

The N K-edge NEXAFS spectra of *m*-MTDATA adsorbed on Au(111) shown in Figure 5 were measured at NI, GI, and NE and compared to the corresponding gas-phase spectrum (14). By contrast to the C K-edge NEXAFS, we observe a strong polarization dependence of the π* and σ* resonances. The main resonance of the adsorbed films (interface and multilayer) is found at 402.42 eV.

For the interface sample, shown in Figure 5c, the π* resonances are enhanced at GI incidence, while the σ* are at NI. Then, as expected, at NE, the NEXAFS features have an intensity between what is observed in the NI and GI spectra. This significant angle ,dependence of the NEXAFS spectra of the interface *m*-MTDATA sample shows that all the planes defined by the N_C–$(C_{ipso})_3$ and N_P–$(C_{ipso})_3$ bonds are almost parallel to the Au(111) surface at this coverage. This means that, although the free *m*-MTDATA is a quite large molecule with phenyl rings and methyl groups twisted and forming a complex molecular structure, when it is adsorbed on the Au(111) surface, the four planes defined by the N_C–$(C_{ipso})_3$ and N_P–$(C_{ipso})_3$ bonds are forced, by the molecule–surface interaction, to be parallel to the Au(111) surface. It is then normal to expect that this molecular rearrangement (unlike the gas-phase structure) has a significant impact on the C 1s and N 1s PES results, as previously discussed.

In Figure 5b, a weaker angle dependence is observed for the multilayer *m*-MTDATA film, showing that the molecular layers become more disordered and that the N_C–$(C_{ipso})_3$ and N_P–$(C_{ipso})_3$ planes are no longer parallel to the surface. Furthermore, the asymmetry tail observed at the lower photon energy side of the π* resonance of the N K-edge NEXAFS spectrum (399.5–402.3 eV) of the multilayer sample, can most likely be attributed to the same transitions contributing to the pre-edge of the gas phase (to LUMO+1 and LUMO+2 having mostly in-plane contribution from the N $2p_{xy}$ component). (14)

For the interface *m*-MTDATA coverage on Au(111) the N K-edge NEXAFS clearly shows an extra broad pre-edge low-intensity feature, between 398 eV and the main resonance (402.42 eV). The new pre-edge feature has an origin different from that observed for the isolated *m*-MTDATA (Figure 5a), considering the following: (i) the new pre-edge covers a wider photon energy range (∼4 eV) than the pre-edge feature in isolated *m*-MTDATA (∼1 eV, Figure 5a); (ii) the angle dependence of the adsorbate NEXAFS spectra of the interface sample reveals that this pre-edge peak can be ascribed to the out-of-plane π orbitals since its intensity grows significantly at GI (especially evident in 399–400 eV in Figure 5c), whereas the pre-edge peak for free *m*-MTDADA was ascribed to transitions involving mostly in-plane (N $2p_{xy}$) orbitals; (14) (iii) this new interface pre-edge feature is almost absent in the multilayer spectrum (Figure 5b), which instead shows only a similar pre-edge feature as for the gas-phase case, at around 401.8 eV.

In summary, the pre-edge feature for the interface sample can be attributed to the molecule–surface interaction. In a previous study about 1,4-benzenediamine (BDA), a similar pre-edge feature was observed and ascribed to N–Au interactions. (35) Our study presents another solid experimental proof for the origin of such pre-edge states due to N–Au interaction. In fact, our study on triphenylamine (TPA) adsorbed on Au(111) suggests a more complex mechanism as the origin of the pre-edge feature, ascribed to the creation of new hybrid states originating from the interaction between the molecule and the gold surface. (34) However, we cannot exclude that core-hole effects during the NEXAFS absorption process could also contribute to the formation of new unoccupied states or to the increase of the strength of the commonly known weak *m*-MTDATA/Au interaction.

Given the electron-donating properties of *m*-MTDATA, and in light of our recent findings regarding the TPA/Au(111) system, we could speculate that the new out-of-plane component observed in the GI N K-edge spectrum for the interface sample (Figure 5c) derives from new available valence states originating from the molecule–surface interaction. These new states are available for new possible electron transitions observed as the pre-edge intensity feature in the N K edge spectrum, as already observed and discussed in our study about TPA/Au(111). Also, the C 1s and N 1s PE BE energy positions on the edge of adsorption resonances (marked as bars in the Figures 4 and 5) confirm a quite significant interaction between the molecule and the surface. (36)

Valence Band PES

To enhance the surface sensitivity, the valence band PES measurements were taken at the NI geometry (i.e., grazing emission). The valence spectra taken with photon energies of 40 and 100 eV of the interface *m*-MTDATA/Au(111) sample are depicted in Figure 6c,d, respectively. In the figure, we also show the VB of clean Au(111) (measured in the same conditions) and the valence PES results of *m*-MTDATA in the gas phase. This allows us to distinguish the molecular valence features from those of the substrate. As expected, the contributions from the substrate dominate the spectrum in the binding energy region between 2 and 8 eV of the VB spectrum taken at 100 eV of the interface sample. On the other hand, the comparison between the isolated and interface samples helps in recognizing the molecular features observed at binding energies >8 eV and at binding energies >6 eV in the spectrum taken with a photon energy of 40 eV. The characteristic three-peak *m*-MTDATA outermost valence feature (14) is quite well resolved, with the HOMO–2 peak a little hidden in the strong Au substrate signal. The *m*-MTDATA HOMO, HOMO–1, and (trace of) HOMO–2 are, respectively, at 0.9, 1.5, and 2.1 eV, keeping the same energy separation of 0.6 eV as in the gas phase.

Similarly, the VB PES results of the multilayer sample of *m*-MTDATA/Au(111) are shown in Figure 6a,b, measured at 40 and 100 eV, respectively. Although the spectrum taken at 100 eV has a large Au(111) substrate contribution in the energy region between 2 and 8 eV, the *m*-MTDATA valence photoemission features are clearly visible, as observed from the similarity to the PES results of *m*-MTDATA measured in the gas phase. The characteristic *m*-MTDATA outermost features are well observed. The HOMO, HOMO–1, and (trace of) HOMO–2 are at 1.08, 1.68, and 2.28 eV, respectively. Compared to the interface sample, these features are shifted (+0.18 eV) to higher binding energy, likely related to a less effective screening effect from the Au(111) substrate for thicker molecular coverages. (25)

The lost resolution for the three expected features in the multilayer spectrum taken with 100 eV photon energy (Figure 6b) can be related to different combined effects. The more bulk sensitive measurements

at such a photon energy (with respect to 40 eV, shown in Figure 6a) affects the spectroscopic results that are the contributions from different molecular layers and from the Au(111) substrate. As also indicated by the N K-edge NEXAFS results, the multilayer sample is characterized by a not ordered molecular arrangement, which would cause a broadening of the spectroscopic lines. Moreover, the experimental resolution using100 eV photon energy is slightly worse than when using 40 eV. In principle, the beam damage could also broaden the peaks, but we carefully checked that the characterized films were not damaged.

Energy Level Alignment

The results of the valence level photoemission for the occupied states and of NEXAFS for the unoccupied states can be aligned, according to the method introduced by Schnadt et al., (37) on a common energy scale, giving an overview of the occupied and unoccupied density of states in the presence of the core-hole. As shown in Figure 7, it is clearly observed that at the interface coverage, the unoccupied N states, i.e., the pre-edge feature of the N K-edge NEXAFS, appear to extend and overlap with the Au Fermi level, confirming the possibility of a charge redistribution channel between the Au surface and the *m*-MTDATA molecule. The hybridization between the molecular orbitals and the metal electronic states gives rise to these new interface states observed as a pre-edge feature in N K-edge NEXAFS. These new states are filling the HOMO–LUMO gap leading to two important consequences: on one side, this can result in an improved charge transfer efficiency through the substrate; on the other side, these states are filling the molecular energy gap so important for many energy conversion applications.

In summary, through the energy alignment of the molecular levels with the bands of the Au substrate, we can expect an effective charge transfer toward the substrate but losing, at interface coverage, the semiconductor energy gap.

Conclusions

When *m*-MTDATA is deposited on Au(111), both the molecular and electronic structures undergo significant modifications. The C 1s PE spectra of *m*-MTDATA for the low-coverage and interface coverage show a significant change of the intensity ratio of the spectral lines with respect to gas-phase results, suggesting a Volmer–Weber (island) type growth for *m*-MTDATA on Au(111) from the early stages of deposition. For the interface sample, NEXFAS results indicate that all the four planes defined by the N_C–$(C_{ipso})_3$ and N_P–$(C_{ipso})_3$ bonds are almost parallel to the surface upon adsorption on Au(111). Moreover, a new pre-edge feature clearly observed in the N K-edge NEXAFS of the interface sample is ascribed to new states formed by the interaction between the molecules and the gold substrate, appearing in the original molecular energy gap. These results have important implications for single molecule devices and 2D layer optoelectronics, which are highly dependent on the molecule–substrate or molecule–electrodes interface. Although the formation of new interface states observed in our study can indicate the possibility of a more effective charge transfer, these states also fill the molecular energy gap, affecting the optical absorption properties of the molecule.

Acknowledgments

We thank the Carl Trygger Foundation for financial support and for making available the VG-Scienta SES-200 photoelectron analyser at the Gas Phase beamline, Elettra, Italy. T.Z. is thankful for the financial

support from the National Natural Science Foundation of China (Nos. 61901038, 61971035, 61725107, 92163206), the Beijing Natural Science Foundation (Nos. Z190006, 4192054), and the National Key Research and Development Program of China (2020YFA0308800, 2019YFA0308000) and the support from the Beijing Institute of Technology Research Fund Program for Young Scholars and the Vice-Chancellor of Uppsala University for financial support through the U4 collaboration. B.B. acknowledges the Swedish Research Council for research grant (VR 2014-3776). F.O.L.J acknowledges support from the Swedish Research Council (grants VR 2014-6463 and 2020-06409). The authors acknowledge the EU CERIC–ERIC Consortium for the access to experimental facilities and financial support. We thank the staff at Materials Science beamline, at Elettra, for all the help provided during the beamtimes. We thank G. Bortoletto and C. Pedersini of the User Support Lab at Elettra. We also thank Prof. N. Mårtensson and Prof. S. Svensson for helpful discussions.

References

[1] Nishimura, K.; Kobata, T.; Inada, H.; Shirota, Y. Arylaldehyde and Arylketone Hydrazones as a New Class of Amorphous Molecular Materials. J. Mater. Chem. 1991, 1 (5), 897, DOI: 10.1039/jm9910100897

[2] Ishikawa, W.; Inada, H.; Nakano, H.; Shirota, Y. Methyl-Substituted Derivatives of 1,3,5-Tris(Diphenylamino)Benzene as a Novel Class of Amorphous Molecular Materials. Chem. Lett. 1991, 20 (10), 1731– 1734, DOI: 10.1246/cl.1991.1731

[3] Higuchi, A.; Inada, H.; Kobata, T.; Shirota, Y. Amorphous Molecular Materials: Synthesis and Properties of a Novel Starburst Molecule, 4,4′,4″ -Tri(N-Phenothiazinyl)Triphenylamine. Adv. Mater. 1991, 3 (11), 549– 550, DOI: 10.1002/adma.19910031105

[4] Ishikawa, W.; Inada, H.; Nakano, H.; Shirota, Y. Starburst Molecules for Amorphous Molecular Materials: Synthesis and Morphology of 1,3,5-Tris(Diphenylamino)Benzene and Its Methyl-Substituted Derivatives. Mol. Cryst. Liq. Cryst. Sci. Technol. Sect. A. Mol. Cryst. Liq. Cryst. 1992, 211 (1), 431– 438, DOI: 10.1080/10587259208025844

[5] Higuchi, A.; Ohnishi, K.; Nomura, S.; Inada, H.; Shirota, Y. Tri(Biphenyl-4-Yl)Amine and Tri(p-Terphenyl-4-Yl)Amine as a Novel Class of Molecules for Amorphous Molecular Materials. J. Mater. Chem. 1992, 2 (10), 1109, DOI: 10.1039/jm9920201109

[6] Inada, H.; Shirota, Y. 1,3,5-Tris[4-(Diphenylamino)Phenyl]Benzene and Its Methyl-Substituted Derivatives as a Novel Class of Amorphous Molecular Materials. J. Mater. Chem. 1993, 3 (3), 319, DOI: 10.1039/jm9930300319

[7] Ishikawa, W.; Noguchi, K.; Kuwabaru, Y.; Shirota, Y. Novel Amorphous Molecular Materials: The Starburst Molecule 1,3,5-Tris[N-(4-Diphenyl- Aminophenyl)Phenylamino]Benzene. Adv. Mater. 1993, 5 (7–8), 559– 561, DOI: 10.1002/adma.19930050709

[8] Naito, K.; Miura, A. Molecular Design for Nonpolymeric Organic Dye Glasses with Thermal Stability: Relations between Thermodynamic Parameters and Amorphous Properties. J. Phys. Chem. 1993, 97 (23), 6240– 6248, DOI: 10.1021/j100125a025

[9] Deotare, P. B.; Chang, W.; Hontz, E.; Congreve, D. N.; Shi, L.; Reusswig, P. D.; Modtland, B.; Bahlke, M. E.; Lee, C. K.; Willard, A. P.; Bulovic, V.; Van Voorhis, T.; Baldo, M. A. Nanoscale Transport of Charge-Transfer States in Organic Donor-Acceptor Blends. Nat. Mater. 2015, 14 (11), 1130– 1134, DOI: 10.1038/nmat4424

[10] Goushi, K.; Adachi, C. Efficient Organic Light-Emitting Diodes through up-Conversion from Triplet to Singlet Excited States of Exciplexes. Appl. Phys. Lett. 2012, 101 (2), 023306, DOI: 10.1063/1.4737006

[11] Wang, S.; Wang, X.; Yao, B.; Zhang, B.; Ding, J.; Xie, Z.; Wang, L. Solution-Processed Phosphorescent Organic Light-Emitting Diodes with Ultralow Driving Voltage and Very High Power Efficiency. Sci. Rep. 2015, 5 (1), 12487, DOI: 10.1038/srep12487

[12] Johansson, E. M. J.; Karlsson, P. G.; Hedlund, M.; Ryan, D.; Siegbahn, H.; Rensmo, H. Photovoltaic and Interfacial Properties of Heterojunctions Containing Dye-Sensitized Dense TiO2 and Tri-Arylamine Derivatives. Chem. Mater. 2007, 19 (8), 2071– 2078, DOI: 10.1021/cm062498v

[13] Johansson, E. M. J.; Odelius, M.; Karlsson, P. G.; Siegbahn, H.; Sandell, A.; Rensmo, H. Interface Electronic States and Molecular Structure of a Triarylamine Based Hole Conductor on Rutile TiO2(110). J. Chem. Phys. 2008, 128 (18), 184709, DOI: 10.1063/1.2913245

[14] Zhang, T.; Brumboiu, I. E.; Lanzilotto, V.; Grazioli, C.; Guarnaccio, A.; Johansson, F. O. L.; Coreno, M.; de Simone, M.; Santagata, A.; Brena, B.; Puglia, C. Electronic Structure Modifications Induced by Increased Molecular Complexity: From Triphenylamine to m-MTDATA. Phys. Chem. Chem. Phys. 2019, 21 (32), 17959– 17970, DOI: 10.1039/C9CP02423A

[15] Shirota, Y.; Kobata, T.; Noma, N. Starburst Molecules for Amorphous Molecular Materials. 4,4′,4″-Tris(N,N-Diphenylamino)Triphenylamine and 4,4′,4″-Tris[N-(3-Methylphenyl)-N-Phenylamino]Triphenylamine. Chem. Lett. 1989, 18, 1145– 1148, DOI: 10.1246/cl.1989.1145

[16] Agarwala, P.; Kabra, D. A Review on Triphenylamine (TPA) Based Organic Hole Transport Materials (HTMs) for Dye Sensitized Solar Cells (DSSCs) and Perovskite Solar Cells (PSCs): Evolution and Molecular Engineering. J. Mater. Chem. A 2017, 5 (4), 1348– 1373, DOI: 10.1039/C6TA08449D

[17] Inada, H.; Ohnishi, K.; Nomura, S.; Higuchi, A.; Nakano, H.; Shirota, Y. Photo- and Electro-Active Amorphous Molecular Materials: Morphology, Structures, and Hole Transport Properties of Tri(Biphenyl-4-Yl)Amine. J. Mater. Chem. 1994, 4 (2), 171, DOI: 10.1039/jm9940400171

[18] Kabe, R.; Adachi, C. Organic Long Persistent Luminescence. Nature 2017, 550 (7676), 384– 387, DOI: 10.1038/nature24010

[19] Wang, J.; Liu, K.; Ma, L.; Zhan, X. Triarylamine: Versatile Platform for Organic, Dye-Sensitized, and Perovskite Solar Cells. Chem. Rev. 2016, 116 (23), 14675– 14725, DOI: 10.1021/acs.chemrev.6b00432

[20] Jailaubekov, A. E.; Willard, A. P.; Tritsch, J. R.; Chan, W. L.; Sai, N.; Gearba, R.; Kaake, L. G.; Williams, K. J.; Leung, K.; Rossky, P. J.; Zhu, X. Y. Hot Charge-Transfer Excitons Set the Time Limit for Charge Separation at Donor/Acceptor Interfaces in Organic Photovoltaics. Nat. Mater. 2013, 12 (1), 66– 73, DOI: 10.1038/nmat3500

[21] Vandewal, K.; Albrecht, S.; Hoke, E. T.; Graham, K. R.; Widmer, J.; Douglas, J. D.; Schubert, M.; Mateker, W. R.; Bloking, J. T.; Burkhard, G. F.; Sellinger, A.; Fréchet, J. M. J.; Amassian, A.; Riede, M. K.; McGehee, M. D.; Neher, D.; Salleo, A. Efficient Charge Generation by Relaxed Charge-Transfer States at Organic Interfaces. Nat. Mater. 2014, 13 (1), 63– 68, DOI: 10.1038/nmat3807

[22] Gelinas, S.; Rao, A.; Kumar, A.; Smith, S. L.; Chin, A. W.; Clark, J.; van der Poll, T. S.; Bazan, G. C.; Friend, R. H. Ultrafast Long-Range Charge Separation in Organic Semiconductor Photovoltaic Diodes. Science (80-.) 2014, 343 (6170), 512– 516, DOI: 10.1126/science.1246249

[23] Cha, H.; Wu, J. Understanding What Determines the Organic Solar Cell Stability. Joule 2021, 5 (6), 1322– 1325, DOI: 10.1016/j.joule.2021.05.020

[24] Müller, K.; Schmidt, N.; Link, S.; Riedel, R.; Bock, J.; Malone, W.; Lasri, K.; Kara, A.; Starke, U.; Kivala, M.; Stöhr, M. Triphenylene-Derived Electron Acceptors and Donors on Ag(111): Formation of Intermolecular Charge-Transfer Complexes with Common Unoccupied Molecular States. Small 2019, 15 (33), 1901741, DOI: 10.1002/smll.201901741

[25] Zhang, T.; Brumboiu, I. E.; Lanzilotto, V.; Lüder, J.; Grazioli, C.; Giangrisostomi, E.; Ovsyannikov, R.; Sassa, Y.; Bidermane, I.; Stupar, M.; de Simone, M.; Coreno, M.; Ressel, B.; Pedio, M.; Rudolf, P.; Brena, B.; Puglia, C. Conclusively Addressing the CoPc Electronic Structure: A Joint Gas-Phase and Solid-State Photoemission and Absorption Spectroscopy Study. J. Phys. Chem. C 2017, 121 (47), 26372– 26378, DOI: 10.1021/acs.jpcc.7b08524

[26] Tsud, N.; Acres, R. G.; Iakhnenko, M.; Mazur, D.; Prince, K. C.; Matolín, V. Bonding of Histidine to Cerium Oxide. J. Phys. Chem. B 2013, 117 (31), 9182– 9193, DOI: 10.1021/jp404385h

[27] Becke, A. D. Density-functional Thermochemistry. III. The Role of Exact Exchange. J. Chem. Phys. 1993, 98 (7), 5648– 5652, DOI: 10.1063/1.464913

[28] Rassolov, V. A.; Pople, J. A.; Ratner, M. A.; Windus, T. L. 6-31G* Basis Set for Atoms K through Zn. J. Chem. Phys. 1998, 109 (4), 1223– 1229, DOI: 10.1063/1.476673

[29] Frisch, M. J.; Trucks, G. W.; Schlegel, H. B.; Scuseria, G. E.; Robb, M. A.; Cheeseman, J. R.; Scalmani, G.; Barone, V.; Petersson, G. A.; Nakatsuji, H.; Li, X.; Caricato, M.; Marenich, A. V; Bloino, J.; Janesko, B. G.; Gomperts, R.; Mennucci, B.; Hratchian, H. P.; Ortiz, J. V; Izmaylov, A. F.; Sonnenberg, J. L.; Williams-Young, D.; Ding, F.; Lipparini, F.; Egidi, F.; Goings, J.; Peng, B.; Petrone, A.; Henderson, T.; Ranasinghe, D.; Zakrzewski, V. G.; Gao, J.; Rega, N.; Zheng, G.; Liang, W.; Hada, M.; Ehara, M.; Toyota, K.; Fukuda, R.; Hasegawa, J.; Ishida, M.; Nakajima, T.; Honda, Y.; Kitao, O.; Nakai, H.; Vreven, T.; Throssell, K.; Montgomery, J. A., Jr.; Peralta, J. E.; Ogliaro, F.; Bearpark, M. J.; Heyd, J. J.; Brothers, E. N.; Kudin, K. N.; Staroverov, V. N.; Keith, T. A.; Kobayashi, R.; Normand, J.; Raghavachari, K.; Rendell, A. P.; Burant, J. C.; Iyengar, S. S.; Tomasi, J.; Cossi, M.; Millam, J. M.; Klene, M.; Adamo, C.; Cammi, R.; Ochterski, J. W.; Martin, R. L.; Morokuma, K.; Farkas, O.; Foresman, J. B.; Fox, D. J. Gaussian 16, Revision B.01; Gaussian Inc.: Wallingford, CT, 2016.

[30] Tillborg, H.; Nilsson, A.; Mårtensson, N. Shake-up and Shake-off Structures in Core Level Photoemission Spectra from Adsorbates. J. Electron Spectrosc. Relat. Phenom. 1993, 62 (1–2), 73–93, DOI: 10.1016/0368-2048(93)80007-9

[31] Totani, R.; Grazioli, C.; Zhang, T.; Bidermane, I.; Lüder, J.; de Simone, M.; Coreno, M.; Brena, B.; Lozzi, L.; Puglia, C. Electronic Structure Investigation of Biphenylene Films. J. Chem. Phys. 2017, 146 (5), 054705, DOI: 10.1063/1.4975104

[32] Graber, T.; Forster, F.; Schöll, A.; Reinert, F. Experimental Determination of the Attenuation Length of Electrons in Organic Molecular Solids: The Example of PTCDA. Surf. Sci. 2011, 605 (9–10), 878–882, DOI: 10.1016/j.susc.2011.01.033

[33] Zhang, T.; Brumboiu, I. E.; Grazioli, C.; Guarnaccio, A.; Coreno, M.; de Simone, M.; Santagata, A.; Rensmo, H.; Brena, B.; Lanzilotto, V.; Puglia, C. Lone-Pair Delocalization Effects within Electron Donor Molecules: The Case of Triphenylamine and Its Thiophene-Analog. J. Phys. Chem. C 2018, 122 (31), 17706– 17717, DOI: 10.1021/acs.jpcc.8b06475

[34] Zhang, T.; Svensson, P. H. W.; Brumboiu, I. E.; Lanzilotto, V.; Grazioli, C.; Guarnaccio, A.; Johansson, F. O. L.; Beranová, K.; Coreno, M.; de Simone, M.; Floreano, L.; Cossaro, A.; Brena, B.; Puglia, C. Clarifying the Adsorption of Triphenylamine on Au(111): Filling the HOMO–LUMO Gap. J. Phys. Chem. C 2022, 126, 1635, DOI: 10.1021/acs.jpcc.1c08877

[35] Balducci, G.; Romeo, M.; Stener, M.; Fronzoni, G.; Cvetko, D.; Cossaro, A.; Dell'Angela, M.; Kladnik, G.; Venkataraman, L.; Morgante, A. Computational Study of Amino Mediated Molecular Interaction Evidenced in N 1s NEXAFS: 1,4-Diaminobenzene on Au (111) -SI. J. Phys. Chem. C 2015, 119 (4), 1988–1995, DOI: 10.1021/jp512146t

[36] Nilsson, A.; Björneholm, O.; Zdansky, E. O. F.; Tillborg, H.; Mårtensson, N.; Andersen, J. N.; Nyholm, R. Photoabsorption and the Unoccupied Partial Density of States of Chemisorbed Molecules. Chem. Phys. Lett. 1992, 197 (1–2), 12– 16, DOI: 10.1016/0009-2614(92)86013-8

[37] Schnadt, J.; O'Shea, J. N.; Patthey, L.; Krempaský, J.; Mårtensson, N.; Brühwiler, P. A. Alignment of Valence Photoemission, x-Ray Absorption, and Substrate Density of States for an Adsorbate on a Semiconductor Surface. Phys. Rev. B 2003, 67 (23), 235420, DOI: 10.1103/PhysRevB.67.235420

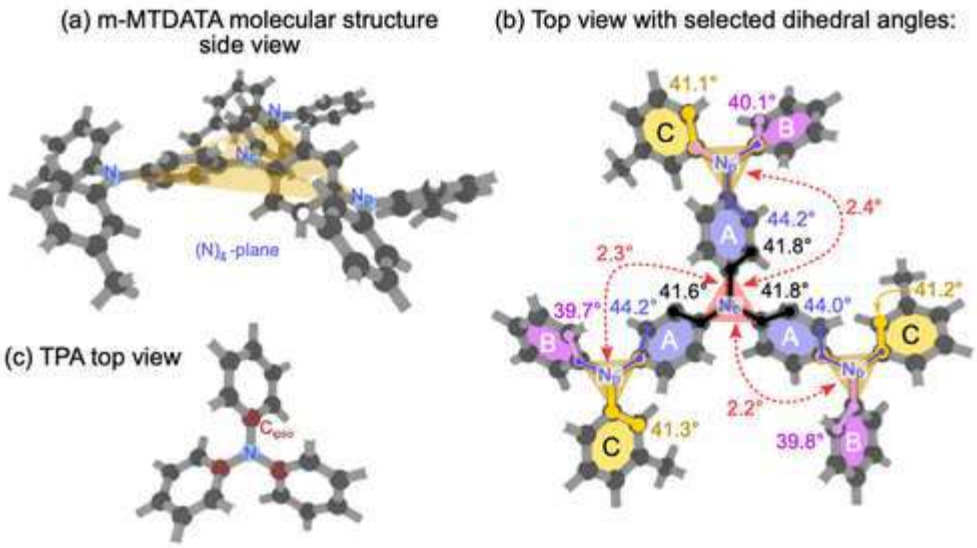

Figure 1. Structure of the *m*-MTDADA (a, b) molecule in comparison to its core molecule TPA (c). (a) Side view of *m*-MTDATA. The 4 N atoms (N_c + 3 N_p) are in the same plane, which defines the molecular N_4-plane of *m*-MTDATA. (b) There are three chemically different phenyl rings (A, B, and C), resulting from the 14 chemically distinct carbon atoms. The torsion angles of the phenyl rings are indicated.

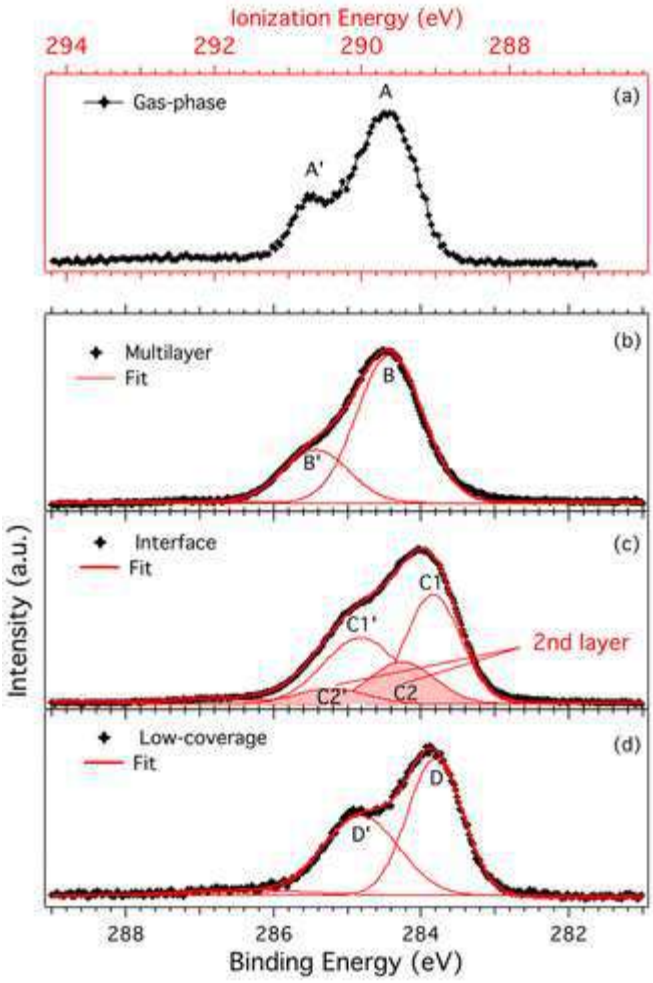

Figure 2. C 1s PE spectra of *m*-MTDATA, showing (a) gas-phase data from ref (14) versus the ionization energy scale (refer to the vacuum level, red axis) and (b)–(d) experimental results and fitting of the C 1s PE spectra (where a Shirley background has been removed) of *m*-MTDATA adsorbed on Au(111) at the indicated different coverage versus a binding energy scale (refer to the Fermi edge, black axis).

456

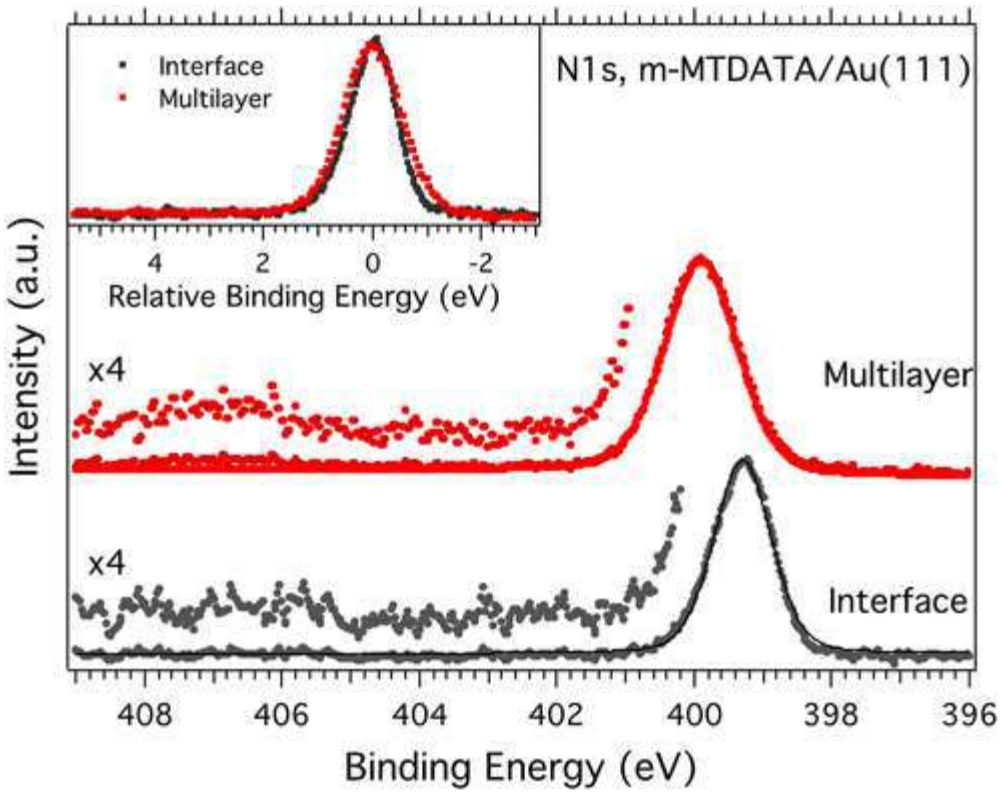

457 **Figure 3.** Comparison between N 1s PE spectra of interface and multilayer coverages of *m*-MTDATA
458 adsorbed on Au(111). In the inset, the comparison of the profiles of the two lines is shown on a relative
459 BE scale.

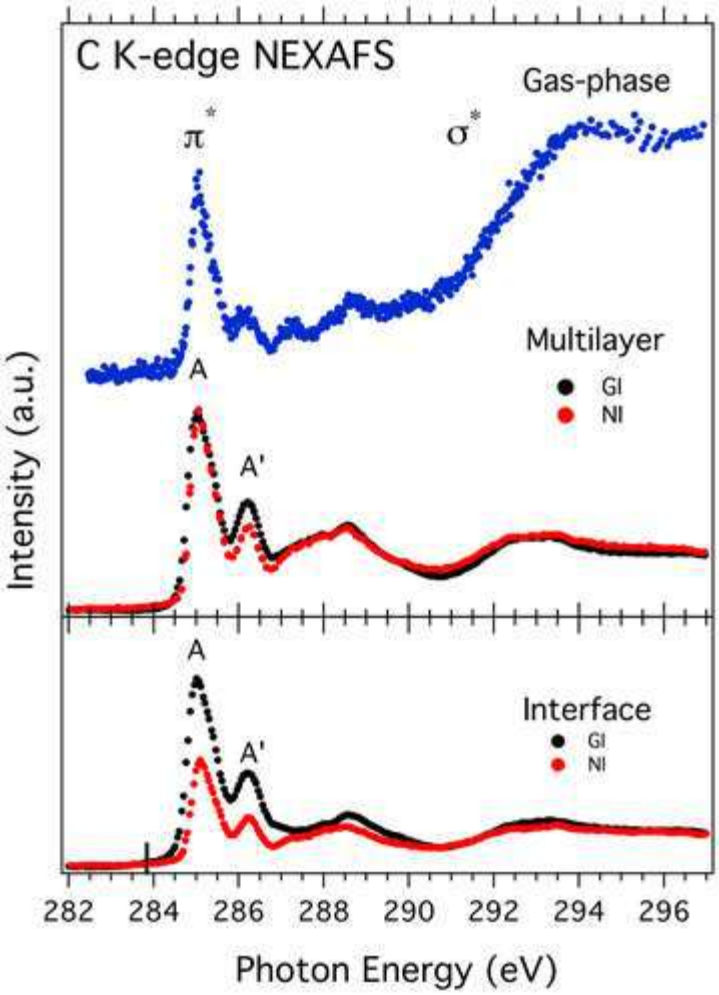

Figure 4. Comparison of the C K-edge NEXAFS of *m*-MTDATA/Au(111) at the interface and multilayer coverages, taken at different experimental setups and compared with the gas-phase results from ref (14). The vertical black bars indicate the binding energy of the corresponding non-ipso phenyl carbon C 1s PES.

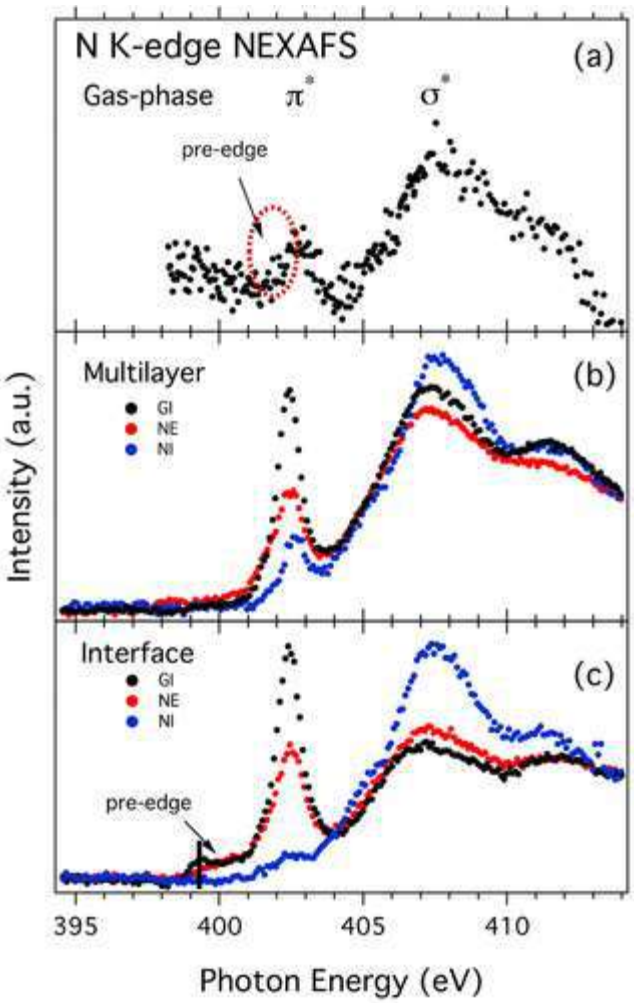

Figure 5. N K-edge NEXAFS spectra of *m*-MTDATA/Au(111) films of interface and multilayer samples, compared to the gas-phase result from ref (14). The vertical black bars indicate the binding energy of the corresponding N 1s PES line.

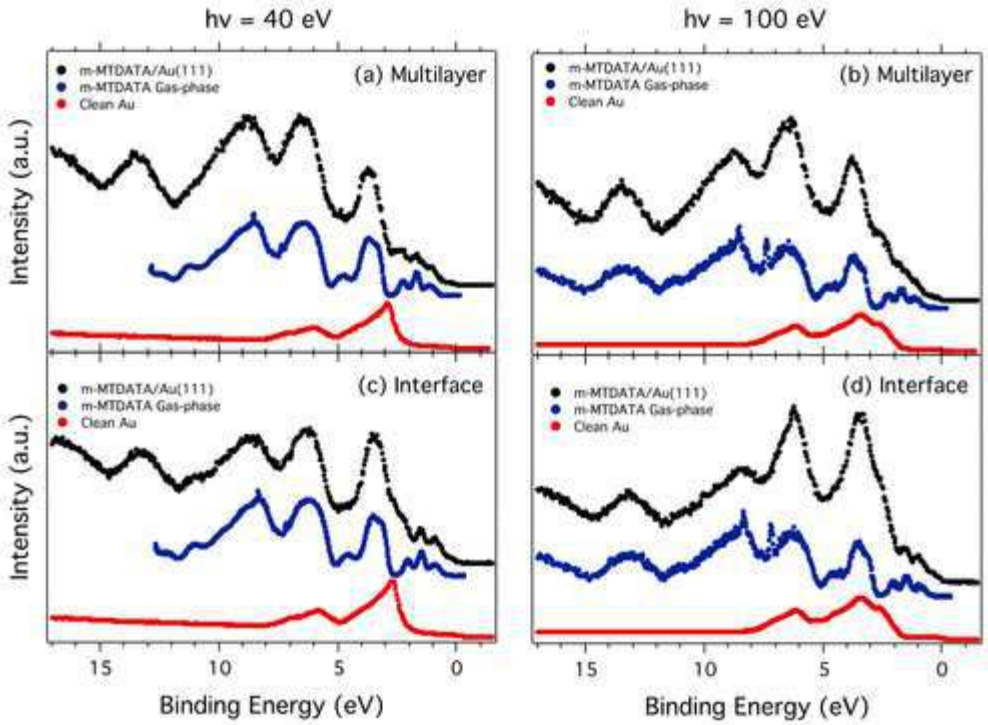

Figure 6. Comparison of valence PE spectra of *m*-MTDATA/Au(111) (blue line with markers) of different thicknesses (multilayer and interface as indicated in the figure) taken at NI, with photon energies of 40 eV (a, c) and 100 eV (b, d). In each panel, the clean Au(111) substrate (black dashed lines) and gas-phase (pink dashed lines, from ref (14)) spectra measured with the same photon energy are also shown. The gas-phase spectrum has been shifted −5.25 eV (−5.45 eV) to align with the multilayer (interface) results.

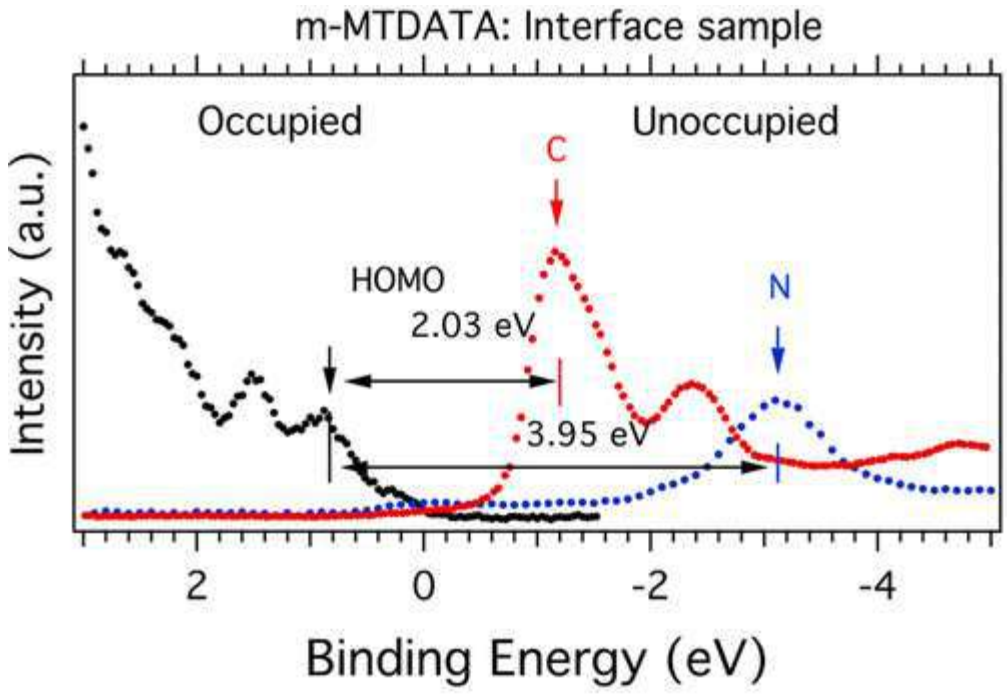

Figure 7. Energy level alignment of the occupied (valence PE results measured at 40 eV) and unoccupied (in the presence of a core hole) (C and N K-edge NEXAFS results) states for *m*-MTDATA/Au at interface sample.

479

Table 1. Fitting Results of C 1s PE Spectra of *m*-MTDATA/Au(111)

	BE (eV)	FWHM (eV)	chemical shift from main peak (eV)	area ratio/main
Multilayer				
main peak (B)	284.43	1.05		
low intensity peak (B′)	285.43	1.13	0.99	2.8
Interface				
main peak (C1)	283.85	0.88		
low intensity peak (C1′)	284.82	1.20	0.98	1.22 (first)
main peak (second layer, C2)	284.25	1.05	0.41	
low intensity peak (second layer, C2′)	285.23	1.10		2.58 (second)
Low Coverage				
main peak (D)	283.82	0.80		
low intensity peak (D′)	284.80	1.20	0.98	1.25

480